Structure of Spinach Nitrite Reductase: Implications for Multi-electron Reactions by the Iron−Sulfur:Siroheme Cofactor[†,‡]

Uma Swamy,[§] Meitian Wang,[§] Jatinda N. Tripathy,[||] Sung-Kun Kim,[||] Masakazu Hirasawa,[||] David B. Knaff,*[,||] and James P. Allen*[,§]

Department of Chemistry and Biochemistry, Arizona State University, Tempe Arizona 85287-1604, and Department of Chemistry and Biochemistry, Texas Tech University, Lubbock, Texas 79409-1061

Received May 25, 2005; Revised Manuscript Received October 5, 2005

ABSTRACT: The structure of nitrite reductase, a key enzyme in the process of nitrogen assimilation, has been determined using X-ray diffraction to a resolution limit of 2.8 Å. The protein has a globular fold consisting of 3 α/β domains with the siroheme−iron sulfur cofactor at the interface of the three domains. The Fe_4S_4 cluster is coordinated by cysteines 441, 447, 482, and 486. The siroheme is located at a distance of 4.2 Å from the cluster, and the central iron atom is coordinated to Cys 486. The siroheme is surrounded by several ionizable amino acid residues that facilitate the binding and subsequent reduction of nitrite. A model for the ferredoxin:nitrite reductase complex is proposed in which the binding of ferredoxin to a positively charged region of nitrite reductase results in elimination of exposure of the cofactors to the solvent. The structure of nitrite reductase shows a broad similarity to the hemoprotein subunit of sulfite reductase but has many significant differences in the backbone positions that could reflect sequence differences or could arise from alterations of the sulfite reductase structure that arise from the isolation of this subunit from the native complex. The implications of the nitrite reductase structure for understanding multi-electron processes are discussed in terms of differences in the protein environments of the cofactors.

Nitrogen assimilation is a fundamental biological process that has marked effects on plant productivity with nitrogen deficiency leading to a decrease in plant growth (*1*−*2*). In oxygenic phototrophs, the pathway for nitrogen assimilation involves two sequential reactions that accomplish the eight-electron reduction of nitrate to ammonia (organisms capable of nitrogen fixation possess an independent pathway that involves the nitrogenase-catalyzed reduction of N_2 to ammonia). Ferredoxin:nitrite oxidoreductase (EC 1.7.7.1), commonly called nitrite reductase, catalyzes the second step in this process, the six-electron reduction of nitrite to ammonia. Ferredoxin-dependent nitrite reductases have been isolated and characterized from a number of higher plants, algae, and cyanobacteria (*3*). All ferredoxin-dependent nitrite reductases contain two prosthetic groups, a siroheme and an iron−sulfur cluster. Sirohemes are reduced porphyrins of the isobacteriochlorin class. In nitrite and sulfite reductases, the sirohemes are axially coordinated through a cysteine residue that also serves as one of the ligands for the iron−sulfur cluster (*3*). Nitrite binds to the iron of the siroheme, at the axial position opposite the iron−sulfur cluster (*4*−*6*). In cyanobacteria and chloroplasts of photosynthetic eukaryotes, the physiological electron-donor ferredoxin is reduced by light-dependent reactions of the electron-transfer chain. In higher plants such as spinach, ferredoxin-dependent nitrite reductase is present both in the chloroplasts and in nonphotosynthetic tissues such as roots, where ferredoxin is reduced by the NADPH pool produced via the reductive pentose phosphate cycle (*7*).

Nitrite reductases are widespread in both eukaryotes and prokaryotes and have critical roles in both nitrogen assimilation and dissimilation. Despite the use of the common name of nitrite reductase, the enzymes participating in assimilation and dissimilation carry out only superficially similar reactions with bacterial dissimilatory nitrite reductases having significantly different protein compositions and cofactors than the assimilatory nitrite reductases. Assimilatory nitrite reductases have a limited sequence homology to another siroheme-containing class of enzymes, assimilatory sulfite reductases, which convert sulfite into sulfide for incorporation into sulfur-containing amino acids and other sulfur-containing biomolecules. Assimilatory sulfite reductases are found in plants, bacteria, and fungi. Sulfite reductases and nitrite reductases can each reduce the substrate of the other enzyme, although each enzyme has a significantly greater affinity for its normal substrates (*8*). In *Escherichia coli*, sulfite reductase is a large oligomer containing eight 66-kDa flavoprotein subunits (or α subunits) and four 64-kDa hemoprotein subunits (or β subunits) yielding a 780-kDa complex. The structure of the sulfite reductase complex is unknown, but the structure of the hemoprotein subunit from *E. coli*, which contains the siroheme and the Fe_4S_4 cluster, has been determined to a resolution limit of 1.6 Å (*9*).

[†] This work has been supported in part by grants from the U.S. Department of Agriculture (2003-02149 to J.P.A.) and U.S. Department of Energy (DE-FG03-99ER20346 to D.B.K.).

[‡] The coordinates and structure factors for the structures reported here are available from the Protein Data Bank, accession code 2AKJ.

* To whom correspondence should be addressed: Telephone: 480-965-8241. Fax: 480-965-2747. E-mail: jallen@asu.edu (J.P.A.); Telephone: 806-742-2468. Fax: 806-742-1289. E-mail: david.knaff@ttu.edu (D.B.K.).

[§] Arizona State University.

[||] Texas Tech University.

10.1021/bi050981y CCC: $30.25
Published on Web 11/15/2005

Many details concerning the chemical mechanisms that occur in the six-electron reduction of nitrite to ammonia remain incompletely understood; for example, the rates of the electron-transfer steps and their coupling to proton transfer have not been established. Interpretation of the kinetic data in terms of enzymatic mechanisms has been limited in considerable part by the lack of a structural framework on which to base detailed molecular models. To provide this missing structural basis for mechanistic insights, we have determined the structure of nitrite reductase from spinach. In spinach, the protein is expressed as a 594 amino acid protein of which the first 32 amino acids serve as a signal peptide that directs the nuclear-encoded protein into the chloroplast and is subsequently cleaved off (*10*−*11*). Spinach contains a single nitrite reductase gene per haploid genome, and the enzyme found in chloroplasts can also be targeted to roots and other nonphotosynthetic tissues. Oxidation−reduction midpoint potential (E_m) values of −370 and −290 mV have been determined for the iron−sulfur cluster and the siroheme, respectively, and electron transfer has been shown to occur from the iron−sulfur cluster to the siroheme (*12*). The structural factors that allow this enzyme to perform the six-electron reaction are discussed. The structure of nitrite reductase is compared to the structure of sulfite reductase hemoprotein, and the implications for understanding multielectron reactions in biological systems are discussed. A preliminary description of the structure has been presented at the 13th International Congress of Photosynthesis (*13*).

MATERIALS AND METHODS

Expression and Purification. Spinach nitrite reductase was produced as a His-tagged recombinant protein expressed from the pET30b-NiR plasmid in *E. coli* (*14*). The *E. coli* cells were co-transformed with the plasmid pKK233-CysG that contains the *cysG* gene encoding the enzyme that catalyzes the rate-limiting step in siroheme biosynthesis (*14*). The His-tagged recombinant enzyme has spectral and activity properties very similar to those of the enzyme isolated from spinach leaf (*14*). The nitrite reductase gene encodes a precursor form of protein containing 594 amino acids, but the first 32 amino acids are cleaved, leaving a mature, chloroplastic form of the protein consisting of residues 33−594. The amino acid numbering used in this paper starts from the beginning of the mature protein in keeping with previous studies (the additional amino acids present in the form used in this study that are added as part of the N-terminal His-tag motif are not included in the numbering). The purification was performed by a Ni^{2+}-affinity column (Hi-Trap chelating HP 5 mL, Amersham) with an elution buffer containing 200 mM imidazole in 250 mM potassium phosphate buffer (pH 7.0). For further purification, spinach ferredoxin affinity and gel-filtration columns were applied as necessary.

Crystallization and Data Collection. The crystals were obtained by using sitting drop vapor diffusion. The protein was at a concentration of 46 mg/mL and mixed in a 5:5 μL ratio with the reservoir solution composed of 50 mM Tris-HCl at pH 8.5, 15% poly(ethylene glycol) 4000, and 0.1 M $MgCl_2$. The trays were set up and incubated at 4 °C. Brown diamond-shaped crystals were obtained after approximately 6−8 weeks with a maximal length of 0.4 mm. Crystals were transferred to a cryoprotectant solution of 50 mM Tris-HCl at pH 8.5, 30% poly(ethylene glycol) 4000, and 0.1 M $MgCl_2$ and cryo-cooled in a nitrogen-gas steam at 110 K. Diffraction data were collected on a Rigaku R-AXIS IV++ image-plate area detector using Cu Kα radiation from a Rigaku RU-200HB rotating-anode X-ray generator. The X-ray source was equipped with an Osmic confocal mirror assembly. Data were collected to a resolution of 2.8 Å, which were then indexed, integrated, and scaled using *d*TREK* (*15*). A platinum derivative that diffracted to 3 Å was obtained by transferring the crystals to a cryoprotectant solution containing 1 mM K_2PtCl_4 and soaking overnight.

Table 1: Data Collection and Final Refinement Statistics[a]

	native	platinum
space group	$P4_12_12$	$P4_12_12$
unit cell parameters (Å)	$a = 129.0$	$a = 129.1$
	$b = 129.0$	$b = 129.1$
	$c = 120.9$	$c = 120.3$
resolution range for refinement (Å)	40.0−2.8	40.0−3.0
total observations	94 931	230 429
unique reflections	24 304	20 641
completeness for range (%)	99.6 (97.1)	99.1 (99.8)
I/σ	4.5 (1.6)	13.7 (7.1)
R_{merge}	12.4 (33.0)	12.6 (31.3)
figure of merit		0.29 SOLVE
		0.69 RESOLVE
number of atoms used in refinement	4300	
protein	4223	
cofactors	71	
water and ions	6	
R (%)	25.0	
R_{free} (%)	30.0	
Ramachandran plot		
most favored region (%)	84.1	
allowed region (%)	15.9	
mean B value of model (Å^2)	38.1	
root-mean-square bond length deviation (Å)	0.013	
root-mean-square bond angles deviation (Å)	1.749	

[a] Values in parentheses are for the last resolution shell (2.9−2.8 Å).

Structural Analysis. The structure was solved by SIRAS, single isomorphous replacement from the platinum derivative combined with native anomalous scattering from the four iron atoms in the Fe_4S_4 cluster of the protein, treated as a single superatom. *SOLVE* (*16*) was used to refine the positions, occupancies, and B factors of the iron and platinum ions and to derive estimates of the protein phases. Phases calculated by *SOLVE* were improved by solvent flattening and density modification using *RESOLVE* (*17*). *RESOLVE* also built an initial model that was then rebuilt with *XFIT* (*18*) using the hemoprotein subunit of sulfite reductase as a guide. The structure was refined against the native data and using *REFMAC* (*19*). A structure appraisal of the final model using *PROCHECK* (*20*) indicated that 83.9% of the non-glycine and nonproline residues were in the most-favored region of the Ramachandran plot and 16.1% were in the allowed or generously allowed regions. A summary of the refinement statistics is given in Table 1. Almost all of the mature protein was found in the electron density, from amino acid residue 22−556, with the only missing residues being the first 21 amino acid residues of the amino-terminus region, the last 6 amino acid residues forming the carboxyl-terminus

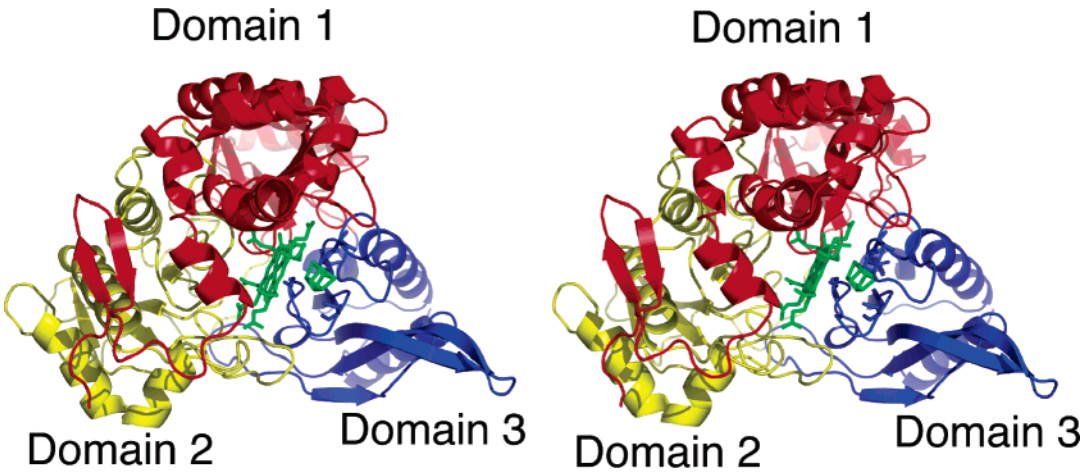

FIGURE 1: Stereoview of the three-dimensional structure of nitrite reductase. The protein is divided into domains 1, formed by residues 22−166 and 353−431 (red), domain 2, formed by residues 167−352 (yellow), and domain 3, formed by residues 432−556 (blue), that surround the central cofactors (green).

region of the protein. All figures are made using PYMOL (*21*).

RESULTS

Structure of Nitrite Reductase. Nitrite reductase is composed of a single polypeptide chain with three domains folded around the cofactors (Figure 1). Domain 1 consists of amino acid residues 22−166 and 353−431, domain 2 consists of residues 167−352, and domain 3 consists of residues 432−556 (Figure 1). Domain 1 has a small region, ending at residue 93, that contains two antiparallel β strands and five small α helices, followed by a region with four α helices and nine β strands, which could be thought as two subdomains (residues 94−166 and 353−431), each containing one β sheet and two α helices, approximately related by a 2-fold symmetry. Domain 2 has a central β sheet surrounded by four α helices and fairly extensive loops. Domain 3 has a central β sheet and two long helices. Together, the domains result in a fairly compact structure, although there are some protruding loops and a set of antiparallel β strands formed by residues 494−517. Certain features of the domains are related to each other by symmetry. One side of the protein is formed by domains 1 and 3, each of which contributes a pair of α helices with each pair roughly symmetrically placed about the center of the protein. Also, the α helices and β sheet of domain 3 can be superimposed upon the corresponding features of domain 2 by a 180° rotation about the center between the two domains. Although these features are approximately symmetrical, the lengths of the α helices and β strands differ and the connecting loops do not maintain the same symmetry.

Buried within the protein are the siroheme and iron−sulfur cluster (Figure 2A). The two cofactors are close together and have a common ligand, Cys 486, that is 2.3 Å from the iron−sulfur cluster and 2.3 Å from the center iron of the siroheme. Surrounding the Fe_4S_4 cluster are two loops formed by amino acid residues 441−447, CTGSQFC, and residues 482−486, with the sequence CPNSC. These four cysteines from these two regions coordinate the iron−sulfur cluster with distances between the iron atoms and cysteine sulfurs around 2.3 Å. These four cysteines had been previously identified, on the basis of conserved sequences found in other proteins that contain Fe_4S_4 clusters, as providing the cluster ligands and shown, by site-directed mutagenesis, to be essential for cofactor binding (*22*).

One of the striking features of the nitrite reductase structure is the presence of seven ionizable residues in close proximity to the siroheme: Arg 98, Arg 109, Arg 143, Arg 149, Arg 223, Lys 224, and Arg 309 (Figure 2B). Presumably, the presence of so many potentially charged residues buried in the protein is due to the requirement of the protein to stabilize the carboxylate groups of the siroheme, bind nitrite, and perform the six-electron-transfer reaction. Interactions between the siroheme and these residues, as well as nearby residues Thr 141, Thr 142, Gln 147, Asn 226, Gln 306, Gln 402, Thr 442, and Gln 488, and main-chain nitrogens of Phe 265, Thr 142, and Thr 442 probably play crucial roles in determining many of the functional properties of this cofactor. In addition, these amino acids are likely to interact with bound substrates in a manner that should contribute to the 100-fold greater affinity of the enzyme for nitrite than for sulfite (*23*, *24*).

The distal side of the siroheme iron does not have any nearby amino acid residues serving as a ligand, with the closest approach of any side chain to the iron being at least 5 Å. The amino acid residues form a large pocket suitable for binding of a substrate, consistent with the results of spectroscopic studies indicating that nitrite binds at this site (*5*, *6*). Contributing to the binding site are four ionizable residues, Arg 109, Arg 149, Arg 179, and Lys 224, that are largely conserved in the sulfite reductase hemoprotein (*9*) as where the equivalent residues, Arg 83, His 123, Arg 153, and Lys 215. The fact that the unusual presence of several amino acid residues is a conserved feature of these two enzymes suggests that these residues play a critical role in the function of the enzyme, including binding of the negatively charged nitrite. Siroheme binding to the protein and the anion-binding site are stabilized by hydrogen bonding and formation of salt bridges to residues Arg 143, Arg 223, and Gln 402 that are conserved as Arg 117, Arg 214, and Gln 396 in the sulfite reductase hemoprotein. There is no binding of an ion or water molecule in lieu of nitrite at this location based on the electron density. The lack of clear density is consistent with nitrite binding in a heterogeneous manner resulting in a broad distribution of nitrite−iron distances (*6*). Only with a significant improvement in the

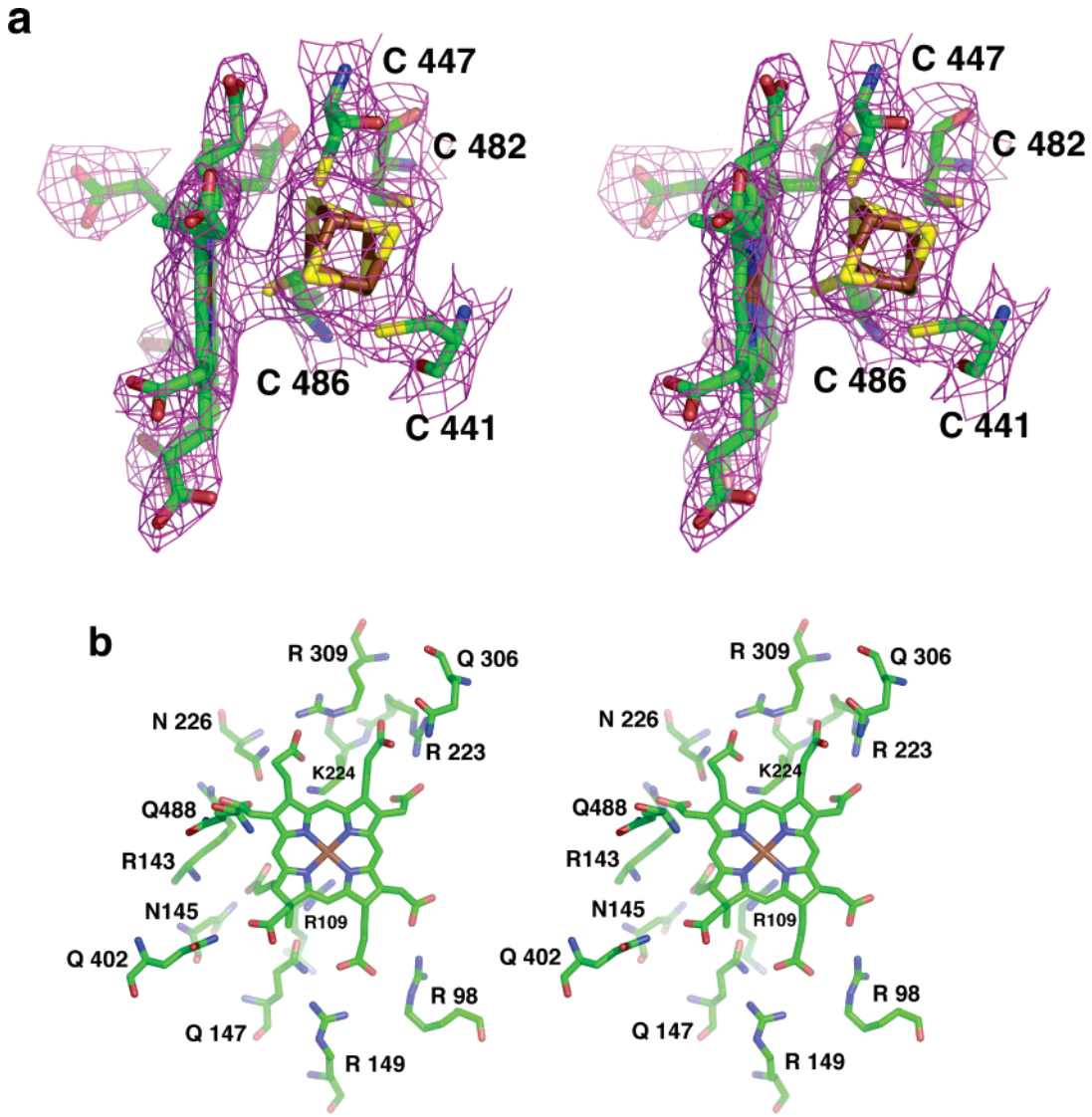

FIGURE 2: Stereoviews of the structural arrangement of the cofactors and nearby residues. (a) Siroheme and iron−sulfur cofactor with the coordinating cysteines, 441, 447, 482, and 486 (carbon, green; oxygen, red; nitrogen, blue; sulfur, yellow; iron, brown). Cys 486 serves as a ligand for both the siroheme iron and the Fe_4S_4 cluster. The $2F_o - F_c$ electron-density map is contoured at a 1σ level. (b) View of the distal position of the siroheme showing the presence of the ionizable amino acid residues Arg 98, Arg 109, Arg 143, Arg 149, Arg 223, Lys 224, and Arg 309 and nearby residues Asn 145, Gln 147, Asn 226, Gln 306, Gln 402, and Gln 486.

resolution limit of the data would a loosely bound ion or water molecule be evident in the electron density.

DISCUSSION

Nitrite reductase is a critical enzyme in the process of nitrogen assimilation. The enzyme binds nitrite to a large cavity region of the protein at the distal position of the siroheme. While electron paramagnetic resonance (EPR)[1] data is equally consistent with the resting enzyme having a five-coordinated siroheme Fe or six-coordinated heme with one weak axial ligand, resonance Raman data are much more consistent with this Fe being six-coordinated with a second but weak axial ligand being present, in addition to the sulfur ligand from Cys 486. In the absence of nitrite, the sixth ligand could be either a weakly bound water molecule or, most likely, a phosphate ion from the buffer (*5*, *6*). The binding of nitrite to the distal position should be stabilized by the presence of several Lys and Arg residues that accommodate the negatively charged nitrite ion. Despite the close distance and common ligand, the siroheme and iron−sulfur cluster act independently, with the iron−sulfur cluster receiving electrons from ferredoxin and transferring them to the siroheme, which in turn transfers them to the substrate, nitrite, that remains bound until its complete reduction to ammonia (*5*, *6*).

Nitrite reductase, as isolated, is fully oxidized, with the cluster in the $(Fe_4S_4)^{2+}$ state and the siroheme iron in the high-spin Fe^{3+} state. The catalytic conversion of nitrite to ammonia occurs via at least five steps. Evidence indicates that, in all likelihood, the enzyme is first reduced by one electron to a state where the siroheme has been reduced to the Fe^{2+} state (the iron−sulfur cluster, although transiently reduced, reverts to the $(Fe_4S_4)^{2+}$ state after reducing the heme), which then binds nitrite rapidly. This adduct is reduced, after the delivery of a second electron, to a NO/ferrosiroheme species, with the cluster in the $(Fe_4S_4)^{2+}$ state.

[1] Abbreviations: EPR, electron paramagnetic resonance.

Addition of two more electrons probably results in reduction of NO to siroheme-bound hydroxylamine (NH_2OH), although the hydroxylamine adduct has not been characterized to date. Finally, two more electrons are added to produce NH_4^+ (*5*, *6*). The intermediate products are retained within the protein until ammonia is formed and released.

These reductions must be coupled to the transfer of protons, because the conversion of nitrite to the ammonium ion and two water molecules requires a total of eight protons. Thus, the distal side of the siroheme must have ready access to protons through either a direct access to the solvent or through a proton pathway involving a series of protonatable amino acid residues that are hydrogen-bonded to each other. An examination of the surface of the protein shows that, despite the general tight packing of the protein, the siroheme and iron−sulfur cluster are located in a tapered channel that has a minimal diameter of approximately 8 Å and leads to the surface of the protein (Figure 3A). Thus, nitrite has a clear path from the surface to the distal side of the siroheme. In turn, ammonia can also readily leave and be replaced by another nitrite molecule while proton transfer is provided directly by the solvent.

Spinach nitrite reductase forms a 1:1 electrostatically stabilized complex with ferredoxin, wherein ferredoxin supplies the negatively charged groups and nitrite reductase supplies the positively charged groups involved in the complex formation (*3*, *25*, *26*). Possible structures of the nitrite reductase:ferredoxin complex were examined by comparing different possible binding pockets of positively charged residues of nitrite reductase that could complement regions of negatively charged residues of spinach ferredoxin 1, the more common isoform found in spinach chloroplasts (PDB code 1A7O; *27*). The initial calculation was performed with FTDOCK, which employs both shape complimentarily using the geometric surface recognition algorithm of Katchalski−Katzir and electrostatic complimentarily to dock two macromolecules (*28*). Because rapid electron transfer from the Fe_2S_2 cluster of the ferredoxin to the Fe_4S_4 cluster of the enzyme requires a favorable distance, the possible outcomes were filtered, so that only those with the smallest distance between the two clusters were considered. This was accomplished by restricting the distances between the Cys 479 and Cys 514 in nitrite reductase and Cys 39 and Cys 44 in ferredoxin to be less than 10 Å (the cofactors were not included in this analysis). The top 200 solutions were refined with MULTIDOCK, a program that refines the interface between two proteins produced by the rigid-body analysis of FTDOCK, including scaling of van der Waals and electrostatic interactions and testing for side-chain conformational changes at the interface (*29*). The 25 most favorable models were inspected with the molecular visualization program XFIT (*18*). Of these 25 solutions, almost all (23) were nearly identical with very small differences of less than 1 Å in the position of the backbone of the ferredoxin relative to nitrite reductase. One of these models was chosen as a representative of the complex and is discussed below in detail. Two of the 25 solutions had comparable energy values with the Fe_2S_2 cluster of the ferredoxin at a nearly identical position, but the ferredoxin was significantly rotated about the Fe_2S_2 cluster relative to the representative model. Thus, the relative positions of the ferredoxin and nitrite reductase in the complex were very comparable for all of the lowest energy models, but the relative orientation of the ferredoxin could not be unambiguously determined.

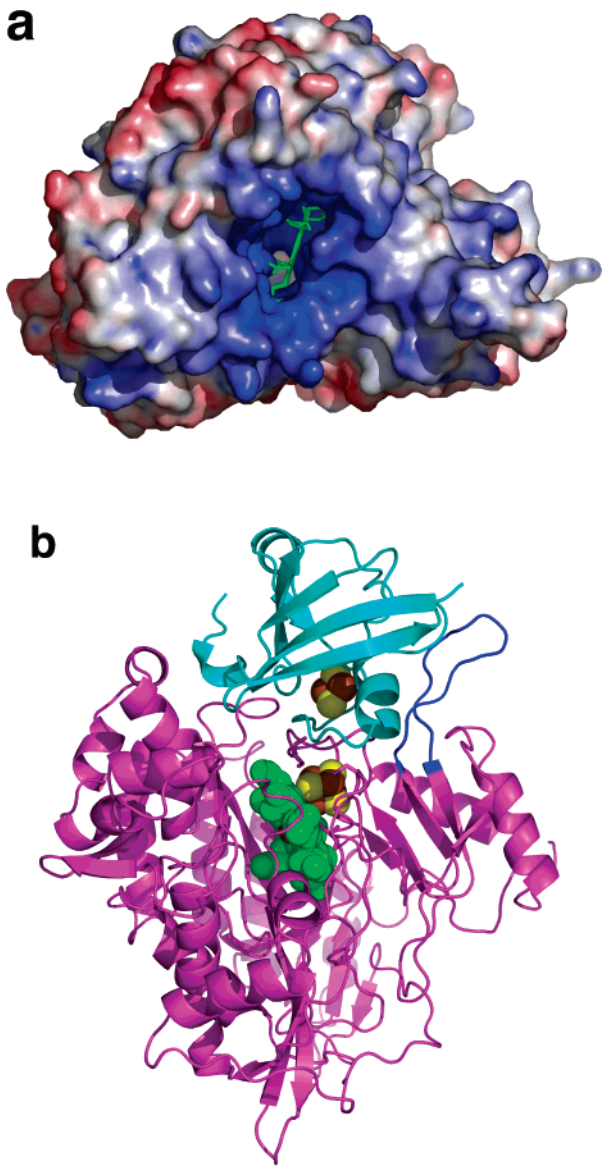

FIGURE 3: Model for the ferredoxin:nitrite reductase complex. (a) Electrostatic surface of nitrite reductase showing the presence of an open tunnel from the surface of the protein to the siroheme and iron−sulfur center. Positive regions are shown as blue, and negative regions are shown as red. Many Lys and Arg are found in this region as shown by the blue shading. (b) Ribbon diagram of the complex of nitrite reductase (purple) and ferredoxin (cyan) with the cofactors shown as space-filling models (siroheme, green; iron, brown; sulfur, yellow). The extended loop formed by amino acid residues 498−512 (dark blue) may help lock in the ferredoxin. The view is rotated by 90° about the horizontal axis relative to the view in a.

In the representative model chosen for the complex (Figure 3B), there are a large number of stabilizing interactions, for example, between Lys 80, 83, 100 of nitrite reductase with Glu 93 and Ser 43 of ferredoxin. Also stabilizing the complex are salt bridges between Arg 502 of nitrite reductase and Asp 60 of ferredoxin and a hydrogen bond from Lys 100 on the enzyme to Ser 43 of ferredoxin. Second, the ferredoxin fits nicely in a pocket of the protein that includes an extension provided by amino acid residues 498−512 that may be able to "lock-in" the ferredoxin upon binding. Third, the ferredoxin fits nicely into the tunnel (Figure 2B). In this

arrangement, the distance from the Fe_2S_2 cluster of the ferredoxin to the Fe_4S_4 cluster of the enzyme is shorter at 11 Å than the 16 Å distance between the Fe_2S_2 cluster of ferredoxin and the siroheme. The shorter distance to the Fe_4S_4 cluster suggests that electron transfer should be significantly faster from the Fe_2S_2 cluster of the ferredoxin to the Fe_4S_4 cluster than to the siroheme, consistent with earlier observations that the Fe_4S_4 cluster is reduced prior to siroheme reduction. In the alternative model, these distances are very comparable and the residues involved in the binding are essentially the same although the specific interactions differ.

Chemical modification studies have been interpreted in terms of the presence of both Arg and Lys residues at the ferredoxin-binding site of nitrite reductase. Peptide-mapping studies implicated three conserved residues, Arg 375, Lys 436, and Arg 556 in ferredoxin binding (*12*, *25*, *30*). These residues are not part of the proposed binding site. Furthermore, these three residues are separated from each other by such large distances that all of these three residues cannot be located at a single ferredoxin-binding site. For the modeling of the complex, it was assumed that the backbone structures of the isolated nitrite reductase and ferredoxin do not change in response to binding. However, it has been shown that complex formation between ferredoxin and nitrite reductase causes changes in the circular dichroism spectra of one or both proteins. These spectroscopic changes are consistent with the hypothesis that protein/protein interactions arising from complex formation result in changes in secondary structure in one or both proteins (*31*) that have not been modeled. The previously observed changes in the chemical modification of these residues because of ferredoxin binding could have occurred because of structural rearrangements of nitrite reductase upon ferredoxin binding. In particular, the strong interactions of ferredoxin with residues 448−451 and 499−510 could result in shifts of the loops formed by residues 430−437, 498−512, and 519−524, following the observed changes in loops evident in the structure of the $NADP^+$ reductase:ferredoxin structure (*32*).

A complex with geometry similar to that shown in Figure 3B provides a possible model for how the protein couples the transfer of eight protons and two water molecules with the six-electron reduction process. The Arg and Lys surrounding the siroheme are unlikely to be all charged because the resulting electrostatic interactions between charges that are 4−8 Å apart would be very unfavorable in the interior of the protein. Rather, the close distances would probably result in large pK_a shifts that result in only some Arg being protonated, most likely those that have a limited solvent exposure such as Arg 223 and Lys 224, because of the solvent located in the channel. When the ferredoxin binds, the channel closes, resulting in the loss of solvent access for the residues near the siroheme. The effect of this desolvation on the mechanism of nitrite to ammonia conversion is not known, but it may contribute because the electron-transfer steps are coupled with proton transfer. This loss of solvent access should result in shifts of the pK_a values of the Arg and Lys residues to lower values and consequently the release of protons. The extent of the pK_a shifts for the residues are difficult to predict because they will depend upon changes in the ionization of nearby residues and dielectric changes in addition to the direct effects of solvent loss. Because the interactions with the surrounding Arg residues should decrease the pK_a values of these residues, the pK_a shift required for deprotonation would not necessarily need to be large to cause proton release. Thus, ferredoxin binding may trigger proton transfer at the same time that electron transfer occurs. Once reduction is complete, the oxidized ferredoxin is released and the pK_a values would be expected to shift back with protons being provided from the bulk solvent.

Comparison to Sulfite Reductase. In addition to sharing an identical set of cofactors, nitrite reductases have limited sequence homology (with sequence identities of approximately 25%) to the hemoprotein subunits of the heterodimeric assimilatory sulfite reductases (*33*). Nitrite reductase contains a single polypeptide chain with ferredoxin serving as an external electron donor. Sulfite reductase from *E. coli* is a large oligomer containing eight copies of the flavoprotein subunit, each with a molecular mass of 66 kDa, and four copies of a hemoprotein subunit, each with a molecular mass of 64 kDa, yielding a 780-kDa complex. The flavoprotein subunit contains iron−sulfur clusters, one FAD and one FMN, all of which participate in transferring electrons from NADPH, the physiological electron donor for the enzyme, to the hemoprotein subunit. The hemoprotein subunit, where substrate reduction occurs, contains one siroheme and one $(Fe_4S_4)^{1+/2+}$ cluster as cofactors. The flavoprotein subunit can be separated from the hemoprotein, and the isolated hemoprotein subunit, although unable to use NADPH as an electron donor, is fully competent to reduce substrates when suitable electron donors such as methyl viologen are provided (*8*).

There are several functional similarities between nitrite reductase and sulfite reductase (*33*). Both nitrite and sulfite reductases employ sirohemes coupled to an Fe_4S_4 cluster to catalyze a six-electron reduction process. They catalyze reduction of the same substrates, i.e., sulfite, nitrite, and hydroxylamine (*23*, *24*, *34*), although each enzyme exhibits a strong catalytic preference for its physiological substrate. In addition to sharing the same prosthetic groups and reducing the same substrates, nitrite reductase and the hemoprotein portion of sulfite reductase are similar in molecular mass (*35*, *36*) and some spectroscopic features (*5*, *6*, *34*, *37*).

A comparison of the structures shows an overall similarity in the folding arrangements but significant differences in the positions of the backbone atoms. In both structures, the siroheme is coupled to the iron−sulfur center through a cysteine that ligates both cofactors. The relative positions and orientations of the siroheme, iron−sulfur cluster, and four-coordinating cysteine ligands are very similar in the two structures, and they can be readily superimposed upon each other, although the loops containing the ligands differ in position by as much as 2 Å. One of the striking differences between the cofactors of nitrite reductase and the sulfite reductase hemoprotein is the much more pronounced planar distortions in the sulfite reductase hemoprotein model. The siroheme of nitrite reductase is very planar with little out-of-plane distortions. In contrast, the siroheme of sulfite reductase hemoprotein has a distinctive ruffled conformation with distortions throughout the macrocycle. The nonplanar features and associated flexibility of the macrocycle have been proposed to play a role in the preference for sulfite binding (*9*). On the basis of studies of isobacteriochlorins,

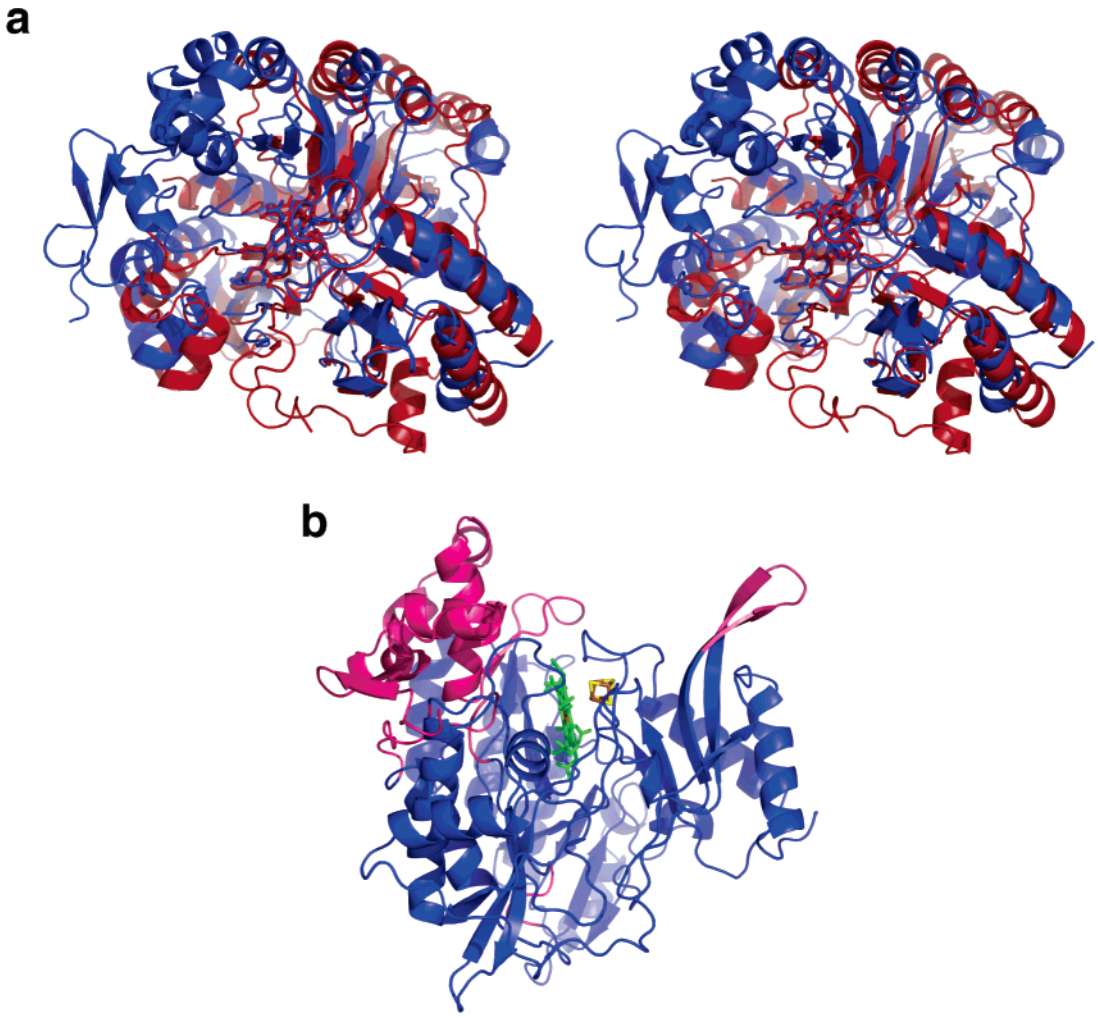

FIGURE 4: Comparison of nitrite reductase and sulfite reductase hemoprotein. (a) Stereoview of the alignment of the structures of nitrite reductase (dark blue) and sulfite reductase hemoprotein (red) based upon the cofactors. Notice the α helices are all shifted in different directions, and the inner portions are more closely aligned. (b) Pink regions of nitrite reductase correspond to the missing or disordered regions of sulfite reductase hemoprotein. Notice that these portions are all localized in one region of nitrite reductase.

these distortions should have significant effects on the electronic structure of the siroheme because the nonplanar distortions destabilize the highest occupied molecular orbitals and consequently should lower the oxidation/reduction potential by 200−300 mV (*38*, *39*). However, the measured difference in the potentials of the sirohemes of nitrite and sulfite reductase is only about 50 mV (*3*). The nonplanar distortions of the sulfite reductase hemoprotein have been proposed to arise from nonuniform protein−cofactor interactions; for example, the siroheme carboxylates form hydrogen bonds that are provided by amino acids from nearby loops (*38*, *39*). The differences in planarity may reflect a combination of factors. While many of these residues are conserved with nitrite reductase, small differences in the interactions may lead to a much more planar siroheme in nitrite reductase. The coordination of the siroheme iron to a strongly bound ion in sulfite reductase but not nitrite reductase should change the out-of-planarity of the central iron atom and hence influence the nonplanar features of the macrocycle. The planarity differences may also reflect different redox states induced by the X-ray radiation during data collection. The details in these planarity differences are currently limited by the resolution limit of the nitrite reductase data because the lack of nonplanar distortions may reflect the resolution of the electron-density maps generated using the nitrite reductase diffraction data. Experiments are underway to improve the quality of the crystals of nitrite reductase to obtain higher resolution data.

Although the cofactors are in relatively similar positions, the model of nitrite reductase and the sulfite reductase hemoprotein shows that the two structures cannot be uniquely aligned nor can the domains be simply shifted relative to each other to align the structures. Superposition of the cofactors shows that the structures are similar for the inner β sheets, but the outer α helices are displaced by 5 Å or more (Figure 4A). The differences may reflect the limited structural homology between nitrite reductase and the sulfite reductase hemoprotein. Most of the differences involve the portions of the sulfite reductase hemoprotein structure that are disordered. In sulfite reductase hemoprotein, residues 1−80 are missing and three regions are disordered: 127−131, 146−148, and 184−209. However, these residues are all located in one region of the protein (Figure 4B), suggesting that the sulfite reductase hemoprotein has "opened up" because of the disorder and missing portions of this region. The opening up largely occurs in the outer regions of the protein because the inner regions are closely aligned, presumably stabilized by the coordination to the cofactors.

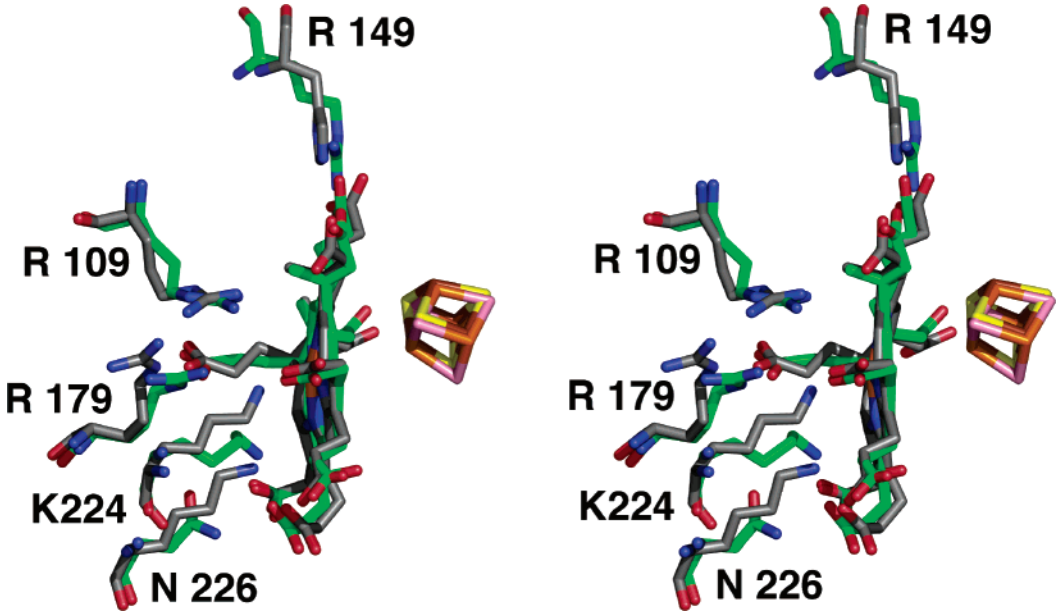

FIGURE 5: Stereoview comparison of the cofactors and distal sides of nitrite reductase and sulfite reductase hemoprotein. Three of the amino acid residues are conserved: Arg 109, Arg 179, and Lys 229 in nitrite reductase (carbon, green; oxygen, red; nitrogen, blue; sulfur, yellow; iron, brown) are equivalent to Arg 83, Arg 153, and Lys 215 (carbon, gray; oxygen, red; nitrogen, blue; sulfur, purple; iron, orange) in the sulfite reductase hemoprotein. Two are not conserved: Arg 149 and Asn 226 in nitrite reductase are equivalent to His 123 and Lys 217 in sulfite reductase hemoprotein.

The substrate in nitrite reductase binds at the distal position of the siroheme as shown by spectroscopic techniques (*4*−*6*). The binding of nitrite to nitrite reductase is relatively weak and disordered compared to the strong binding evident for sulfite reductase (*6*). The superposition of the structures of nitrite reductase and sulfite reductase hemoprotein provides an opportunity to determine the structural reasons for the difference in substrate binding. The overall amino acid conservation is relatively low at 25% identity, giving rise to many differences in the amino acid composition at key secondary-structure elements that contribute to relative shifts of the backbone positions as discussed above. The backbone shifts are evident near the distal site of the siroheme, but there are also residues not conserved in the vicinity. In some cases, the changes are probably minor; for example, Ile 241 and Val 400 in nitrite reductase are equivalent to other aliphatic amino acid residues Ala 232 and Ala 394 in sulfite reductase hemoprotein. In other cases, the changes are more significant; for example, Thr 142 and His 238 in nitrite reductase are located at positions equivalent to Asn 116 and Asp 229 in sulfite reductase hemoprotein. The limited conservation of amino acid residues also results in changes in the charge distribution at the distal side. Four ionizable amino acid residues have been implicated as playing critical roles in substrate binding and establishment of the electrostatic environment in sulfite reductase hemoprotein based on the structures with different bound substrates (*40*). Three of these residues are conserved in the two structures, with Arg 109, Arg 179, and Lys 224 in nitrite reductase equivalent to Arg 83, Arg 153, and Lys 215 in sulfite reductase hemoprotein (Figure 5). One of the residues, Lys 217, that was shown to bind to both sulfite and nitrite in sulfite reductase hemoprotein is not conserved, having been replaced by Asn 226 in nitrite reductase. The binding of nitrite in nitrite reductase must be different both because of the difference in bonding arrangements as well as because of differences in the electrostatic environments as a result of the lack of a Lys at that position. The differences in amino acids are also expected to contribute to the possible differences in planarity of the siroheme in the two structures. For example, the ionizable residue Arg 149 is immediately adjacent to one of the carboxylates of the siroheme in nitrite reductase, but His 123 is located at the equivalent position in sulfite reductase hemoprotein (Figure 5).

SUMMARY

The three-dimensional structure of nitrite reductase has been solved, showing the molecular arrangement of the cofactors and the surrounding protein, and represents the first determination of an assimilatory nitrite reductase. This structure provides the foundation for a molecular understanding of the critical step of nitrogen assimilation, namely, the conversion of nitrite to ammonia. The enzymatic reduction of nitrite to ammonia is an unusual six-electron reduction process (*5*, *6*) that appears to involve the participation of a cluster of ionizable amino acids. Mutational studies of these residues should allow the delineation of the various intermediate steps as well as the coupling of protons to the transfer of electrons. Together with the model of the ferredoxin:nitrite reductase complex, these studies provide a template for multi-electron reactions in other biological systems. For example, the reduction of sulfite to sulfide is catalyzed by the assimilatory ferredoxin-dependent sulfite reductases found in oxygenic phototrophs (*23*, *24*, *41*). The spectroscopic and catalytic properties of these enzymes suggest that they may exhibit a more significant structural homology to nitrite reductase than the bacterial sulfite reductase. Another enzyme that performs multi-electron reductions is nitrogenase, which catalyzes the reduction of dinitrogen to ammonia (*42*, *43*). Clearly, many structural features differ such as the chemical nature of the metal complexes, and only nitrogenase is capable of catalyzing the reduction of dinitrogen. However, these studies of nitrite

reductase may provide insight into how electron transfer is coupled to proton transfer in ferredoxin-driven complexes.

NOTE ADDED IN PROOF

The structure of a ferredoxin-dependent sulfite reductase NirA has been recently reported (*44*).

REFERENCES

1. Poulton, J. E., Romeo, J. T., and Conn, E. E., Eds. (1989) *Plant Nitrogen Metabolism*, Plenum Press, New York.
2. Lea, P. J., and Leegood, R. C., Eds. (1993) *Plant Biochemistry and Molecular Biology*, Wiley, Chichester, U.K.
3. Knaff, D. B. (1996) Ferredoxin and ferredoxin-dependent enzymes, in *Oxygenic Photosynthesis*: *The Light Reactions* (Ort, D. R., and Yocum, C. F., Eds.) pp 333−361, Kluwer Publishers, Dordrecht, The Netherlands.
4. Knaff, D. B., and Hirasawa, M. (1991) Ferredoxin-dependent chloroplast enzymes, *Biochim. Biophys. Acta 1056*, 93−125.
5. Kuznetsova, S., Knaff, D. B., Hirasawa, M., Lagoutte, B., and Setif, P. (2004) Mechanism of spinach chloroplast ferredoxin-dependent nitrite reductase: Spectroscopic evidence for intermediate states, *Biochemistry 43*, 510−517.
6. Kuznetsova, S., Knaff, D. B., Hirasawa, M., Setif, P., and Mattioli, T. A. (2004) Reactions of spinach nitrite reductase with its substrate, nitrite, and a putative intermediate hydroxylamine, *Biochemistry 43*, 10765−10774.
7. Hirasawa, M., Fukushima, K., Tamura, G., and Knaff D. B. (1984) Immunological characterization of nitrite reductases from spinach leaves, spinach roots, and other higher plants, *Biochim. Biophys. Acta 791*, 145−154.
8. Crane, B. R., and Getzoff, E. D. (1996) The relationship between structure and function for the sulfite reductases, *Curr. Opin. Struct. Biol. 6*, 744−756.
9. Crane, B. R., Siegel, L. M., and Getzoff, E. D. (1995) Sulfite reductase structure at 1.6 Å: Evolution and catalysis for reduction of inorganic anions, *Science 270*, 59−67.
10. Back, E., Burkhart. W., Moyer, M., Privalle, L., and Rothstein, S. (1988) Isolation of cDNA clones coding for spinach nitrite reductase: Complete sequence and nitrite induction, *Mol. Gen. Genet. 212*, 20−26.
11. Back, E., Dunne, W., Schneiderbauer, A., de Framond, A., Rastogi, R., and Rothstein, S. J. (1991) Isolation of the spinach nitrite reductase gene promoter which confers nitrite inducibilty on GUS gene expression in transgenic tobacco, *Plant Mol. Biol. 17*, 9−18.
12. Hirasawa, M., Tollin, G., Salamon, Z., and Knaff, D. B. (1994) Transient kinetic and oxidation−reduction studies of spinach ferredoxin:nitrite oxidoreductase, *Biochim. Biophys. Acta 1185*, 336−345.
13. Hirasawa, M., Kuznetsova, S., Sétif, P., Mattioli, T., Tripathy, J., Kim, S.-K., Swamy, U., Wang, M., Allen, J. P., and Knaff, D. B. (2005) Structural, mechanistic, and spectroscopic studies of spinach nitrite reductase, in *Proceedings of the 13th International Congress of Photosynthesis*, pp 825−827, Elsevier Publishers, Amsterdam, the Netherlands.
14. Tripathy, J. N. (2004) The effects of site-directed mutation on spinach nitrite reductase, M.S. Thesis, Texas Tech University, Lubbock, Texas.
15. Pflugrath, J. W. (1999) The finer things in X-ray diffraction data collection, *Acta Crystallogr., Sect. D: Biol. Crystallogr. 55*, 1718−1725.
16. Terwilliger, T. C., and Berendzen, J. (1999) Automated MAD and MIR structure solution, *Acta Crystallogr., Sect. D: Biol. Crystallogr. 55*, 849−861.
17. Terwilliger, T. C. (2003) Automated main-chain model-building by template-matching and iterative fragment extension, *Acta Crystallogr., Sect. D: Biol. Crystallogr. 59*, 38−44.
18. McRee, D. E. (1993) *Practical Protein Crystallography*, Academic Press, San Diego, CA.
19. Murshudov, G. N., Vagin, A. A., and Dodson, E. J. (1997) Refinement of macromolecular structures by the maximum-likelihood method, *Acta Crystallogr., Sect. D: Biol. Crystallogr. 53*, 240−255.
20. Laskowski, R. A., MacArthur, M. W., Moss, D. S., and Thornton, J. M. (1993) Procheck: A program to check the stereochemical quality of protein structures, *J. Appl. Crystallogr. 26*, 283−291.
21. DeLano, W. L. (2002) *The PyMOL Molecular Graphics System*, DeLano Scientific, San Carlos, CA.
22. Bellissimo, D. B., and Privalle, L. S. (1995) Expression of spinach nitrite reductase in *Escherichia coli*: Site-directed mutagenesis of predicted active site amino acids, *Arch. Biochem. Biophys. 323*, 155−163.
23. Krueger, R. J., and Siegel, L. M. (1982) Evidence for siroheme−Fe_4S_4 interaction in spinach ferredoxin-sulfite reductase, *Biochemistry 21*, 2905−2909.
24. Krueger, R. J., and Siegel, L. M. (1982) Spinach siroheme enzymes: Isolation and characterization of ferredoxin-sulfite reductase and comparison of properties with ferredoxin-nitrite reductase, *Biochemistry 21*, 2892−2904.
25. Hirasawa, M., and Knaff, D. B. (1985) Interaction of ferredoxin-linked nitrite reductase with ferredoxin, *Biochim. Biophys. Acta 830*, 173−180.
26. Mikami, B., and Ida, S. (1989) Spinach ferredoxin nitrite reductase: Characterization of catalytic activity and interaction of the enzyme with substrates, *J. Biochem. 105*, 47−50.
27. Binda, C., Coda, A., Aliverti, A., Zanetti, G., and Mattevi, A. (1998) Structure of the mutant E92K of [2Fe−2S] ferredoxin 1 from *Spinacia oleracea* at 1.7 Å resolution, *Acta Crystallogr., Sect. D: Biol. Crystallogr. 54*, 1353−1358.
28. Gabb, H. A., Jackson, R. M., and Sternberg, J. E. (1997) Modelling protein docking using shape complementarity, electrostatics and biochemical information, *J. Mol. Biol.. 272*, 106−120.
29. Jackson, R., Gabb, H. A., and Sternberg, M. J. E. (1998) Rapid refinement of protein interfaces incorporating solvation: Application to the docking problem, *J. Mol. Biol. 276*, 265−285.
30. Dose, M. M., Hirasawa, M., Kleis-SanFrancisco, S., Lew, E. L., and Knaff, D. B. (1997) The ferredoxin-binding site of ferredoxin: Nitrite oxidoreductase, *Plant. Physiol. 114*, 1047−1053.
31. Hirasawa, M., de Best, J. H., and Knaff, D. B. (1993) The effect of lysine- and arginine-modifying reagents on spinach ferredoxin: Nitrite oxidoreductase, *Biochim. Biophys. Acta 1140*, 304−312.
32. Kurisu, G., Kusunoki, M., Katoh, E., Yamazaki, T., Teshima, K., Onda, Y., Kimata-Ariga, Y., and Hase, T. (2001) Structure of the electron-transfer complex between ferredoxin and ferredoxin-$NADP^+$ reductase, *Nat. Struct. Biol. 8*, 117−121.
33. Ostrowski, J., Wu, J. Y., Rueger, D. C., Miller, B. E., Siegel, L. M., and Kredich, N. M. (1989) Characterization of the cysJIH regions of *Salmonella typhimurium* and *Escherichia coli* B. DNA sequences of cysI and cysH and a model for the siroheme−Fe_4S_4 active center of sulfite reductase hemoprotein based on amino acid homology with spinach nitrite reductase, *J. Biol. Chem. 264*, 15726−15737.
34. Siegel, L. M., Rueger, D. C., Barber, M. J., Kreuger, R. J., Orme-Johnson, N. R., and Orme-Johnson, W. H. (1982) *Escherichia coli* sulfite reductase hemoprotein subunit. Prosthetic groups, catalytic parameters, and ligand complexes, *J. Biol. Chem. 257*, 6343−6350.
35. Vega, J. M., and Kamin, H. (1977) Spinach nitrite reductase. Purification and properties of a siroheme-containing enzyme, *J. Biol. Chem. 252*, 896−909.
36. Ida, S., and Mikami, B. (1986) Spinach ferredoxin-nitrite reductase: A purification procedure and characterization of chemical properties, *Biochim. Biophys. Acta 871*, 167−176.
37. Wilkerson, J. O., Janick, P. A., and Siegel, L. M. (1983) Electron paramagnetic resonance and optical spectroscopic evidence for interaction between siroheme and tetranuclear iron−sulfur center prosthetic groups in spinach-ferredoxin nitrite reductase, *Biochemistry 22*, 5048−5054.
38. Crane, B. R., Siegel, L. M., and Getzoff, E. D. (1997) Structures of the siroheme and Fe_4S_4 containing active center of sulfite reductase in different states of oxidation: Heme activation via reduction-gated exogenous ligand exchange, *Biochemistry 36*, 12101−12119.
39. Crane, B. R., Siegel, L. M., and Getzoff, E. D. (1997) Probing the catalytic mechanism of sulfite reductase by X-ray crystallography: Structures of the *Escherichia coli* hemoprotein in complex with substrates, inhibitors, intermediates, and products, *Biochemistry 36*, 12120−12137.
40. Stroupe, M. E., and Getzoff, E. D. (2001) Sulfite reductase hemoprotein, in *Handbook of Metalloproteins* (Messerschmidt, A., Huber, R., Poluos, T., and Wieghart, K., Eds.) pp 471−485, John Wiley and Sons, Chichester, U.K.

41. Nakayama, M., Akashi, T., and Hase, T. (2000) Plant sulfite reductase: Molecular structure, catalytic function, and interaction with ferredoxin, *J. Inorg. Biochem. 82*, 27−32.
42. Rees, D. C., and Howard, J. B. (2000) Nitrogenase: Standing at the crossroads, *Curr. Opin. Chem. Biol. 4*, 559−566.
43. Christiansen, J., Dean, D. R., and Seefeldt, L. C. (2001) Mechanistic features of the Mo-containing nitrogenase, *Annu. Rev. Plant Physiol. Plant Mol. Biol. 52*, 269−295.
44. Schnell, R., Sandalova, T., Hellman, U., Lindqvist, Y., and Schneider, G. (2005) Siroheme- and [Fe_4-S_4]-dependent NirA from *Mycobacterium tuberculosis* is a sulfite reductase with a covalent cys-tyr bond in the active site. *J. Biol. Chem. 280*, 27319−27328.

BI050981Y